Journal of Crohn's and Colitis, 2019, 1186–1200
doi:10.1093/ecco-jcc/jjz039
Advance Access publication April 11, 2019
Original Article

Original Article

The Oxysterol Synthesising Enzyme CH25H Contributes to the Development of Intestinal Fibrosis

T. Raselli,[a] A. Wyss,[a] M. N. Gonzalez Alvarado,[a] B. Weder,[a] C. Mamie,[a] M. R. Spalinger,[a] W. T. van Haaften,[a,b] G. Dijkstra,[b] A. W. Sailer,[c] P. H. Imenez Silva,[d] C. A. Wagner,[d] V. Tosevski,[e] Sebastian Leibl,[f] M. Scharl,[a] G. Rogler,[a] M. Hausmann,[a*] B. Misselwitz[a*]

[a]Department of Gastroenterology and Hepatology, University Hospital Zurich, Zurich University, Zurich, Switzerland [b]Department of Gastroenterology and Hepatology, University Medical Center Groningen, University of Groningen, Groningen, The Netherlands [c]Chemical Biology & Therapeutics, Novartis Institutes for BioMedical Research, Basel, Switzerland [d]Institute of Physiology, Zurich University, Zurich, Switzerland [e]Mass Cytometry Facility, Zurich University, Zurich, Switzerland [f]Institute of Pathology and Molecular Pathology, University Hospital Zurich and Zurich University, Zurich, Switzerland

*MH and BM contributed equally to this work.

Corresponding author: Dr. Benjamin Misselwitz, Dept. of Visceral Surgery and Medicine, Inselspital Bern and Bern University, Freiburgstr 18, 3010 Bern, Switzerland. Email: benjamin.misselwitz@insel.ch

Abstract

Intestinal fibrosis and stenosis are common complications of Crohn's disease [CD], frequently requiring surgery. Anti-inflammatory strategies can only partially prevent fibrosis; hence, anti-fibrotic therapies remain an unmet clinical need. Oxysterols are oxidised cholesterol derivatives with important roles in various biological processes. The enzyme cholesterol 25-hydroxylase [CH25H] converts cholesterol to 25-hydroxycholesterol [25-HC], which modulates immune responses and oxidative stress. In human intestinal samples from CD patients, we found a strong correlation of *CH25H* mRNA expression with the expression of fibrosis markers. We demonstrate reduced intestinal fibrosis in mice deficient for the CH25H enzyme, using the sodium dextran sulphate [DSS]-induced chronic colitis model. Additionally, using a heterotopic transplantation model of intestinal fibrosis, we demonstrate reduced collagen deposition and lower concentrations of hydroxyproline in CH25H knockouts. In the heterotopic transplant model, CH25H was expressed in fibroblasts. Taken together, our findings indicate an involvement of oxysterol synthesis in the pathogenesis of intestinal fibrosis.

Key Words: Fibrogenesis; intestinal fibrosis; cholesterol 25 hydroxylase [CH25H]; oxysterols; transplantation; graft; mouse model

1. Introduction

Crohn's disease [CD] is a major form of inflammatory bowel disease [IBD], characterised by chronic discontinuous inflammatory lesions. Inflammation in CD is typically transmural and can affect the whole gastrointestinal tract, with a preference for the small intestine. Common complications in CD patients include perforations of the gut wall [fistulae and abscesses] as well as intestinal fibrosis and strictures with narrowing of the intestinal lumen. More than 60% of CD patients have to undergo surgery within 20 years following the initial diagnosis,[1] and recurrent disease requires more surgical

procedures in at least 50% of the patients after the first operation.[2,3] The second major form of IBD, ulcerative colitis [UC], characterised by continuous inflammatory lesions of the colon, has been considered a non-fibrotic disease; but recent evidence indicates some degree of submucosal fibrosis in up to 100% of UC colectomy specimens,[4,5] and the degree of fibrosis seems to be proportional to the degree of chronic but not active inflammation.[6]

Currently, no drugs have been approved for treatment or prevention of intestinal fibrosis.[7,8] Anti-inflammatory medications, including anti-tumour necrosis factor [TNF] antibodies or immunosuppressants, are only partially effective in preventing fibrosis,[9] and new preventive and therapeutic strategies are therefore urgently needed.

On a molecular level, fibrosis is characterised by excessive accumulation of extracellular matrix [ECM] components including collagen and laminin, replacing the original tissue and leading to stiffening and loss of normal function.[10,11] Transforming growth factor-β [TGF-β] is a key driver of fibrosis, promoting differentiation of fibroblasts to myofibroblasts, indicated by expression of α-smooth muscle actin [SMA].[12,13] Myofibroblasts are the main effector cells for fibrosis and mainly responsible for ECM deposition.[14–16] On the other hand, myofibroblasts also synthesise matrix metalloproteinases [MMPs] as ECM-degrading enzymes, and their inhibitors [tissue inhibitors of MMPs, TIMPs]. Myofibroblasts can derive from the local fibroblast pool; however, epithelial, endothelial, haematopoietic cells, or pericytes can also differentiate into myofibroblasts.[16] Nevertheless, the chain of events leading to intestinal fibrosis is insufficiently understood.

Studying the pathophysiology of intestinal fibrosis has been limited by the lack of a *bona fide* animal model. Chronic dextran sodium sulphate [DSS] colitis is frequently used as a fibrosis model,[17,18] even though key aspects of CD-associated intestinal fibrosis, such as occlusion of the intestinal lumen, are not observed in this model. Recently, we established and characterised a murine heterotopic transplant model, where small intestinal sections are transplanted into the neck fold of recipient mice.[19,20] In the transplanted sections, the lumen progressively occludes, accompanied by expression of TGF-β and α-SMA as well as collagen deposition in the extracellular matrix. In this model, we previously demonstrated that pirfenidone, an anti-inflammatory and anti-fibrotic drug approved for the treatment of idiopathic pulmonary fibrosis, was able to reduce fibrosis.[20]

Oxysterols are increasingly recognised as immune-modulatory molecules. 25-Hydroxycholesterol [25-HC] is part of the rapid innate immune response and an efficient defence molecule. 25-HC can induce macrophage activation,[21–23] T cell differentiation,[24] and production of IL-8[25–27] as well as IL-6,[23] and was shown to have strong antiviral activity against many enveloped viruses.[28–30] Furthermore, Dang and colleagues recently demonstrated a critical role of 25-HC in inhibiting activation of the DNA sensor protein AIM2, preventing spurious AIM2 inflammasome activation.[31] Cholesterol 25-hydroxylase [CH25H] is the key enzyme mediating hydroxylation of cholesterol to 25-HC.[32] 25-HC is rapidly produced *in vivo* upon immune stimulation by toll-like receptor [TLR] agonists including lipopolysaccharide [LPS] and poly[I:C].[28,30,33,34] 25-HC production was shown to be increased in the airways of patients with chronic obstructive pulmonary disease [COPD] and correlated with the degree of neutrophilic infiltration.[35] 25-HC can be further hydroxylated to di-hydroxy cholesterols [e.g., 7α, 25-HC] which have been shown to act as chemoattractants for cells of the adaptive and innate immune system.[36,37]

Recently, CH25H expression was shown to be upregulated in primary lung fibroblasts in response to activated eosinophils, suggesting CH25H activation in chronic lung diseases including COPD.[38] Profibrotic effects of the CH25H product 25-HC have been demonstrated *in vitro*. In a tissue culture model using human fetal lung fibroblasts [HLF], 25-HC induced nuclear factor-κB [NF-κB] activation with subsequent release of TGF-β, leading to myofibroblast formation, MMP-2 and 9 release, SMA expression, and collagen production.[39] However, the role of 25-HC in intestinal inflammation and fibrosis has not been addressed. In this study, we aimed to investigate the role of the enzyme CH25H in the development of intestinal fibrosis.

2. Materials and Methods

2.1. Human tissue from patients with CD and controls

Intestinal tissue was obtained from patients with CD undergoing ileocaecal resection due to stenosis in the terminal ileum. Non-fibrotic samples originate from the margin of the resections and fibrotic samples from the thickened fibrosis-affected region. Healthy control samples were obtained from patients undergoing right-sided hemicolectomy due to adenocarcinoma [non cancer-affected ileal resection margin]. A power analysis demonstrated that seven cases with a score of 4 [standard deviation of 2] and five controls with a score of 1 [standard deviation of 0.5] would have 90% power to detect this difference at a significance level of 0.05 with a Mann-Whitney U test in a one-sided analysis [G*Power Version 3.1.9.2].[40]

Immediately after resection, samples were fixed in Tissue-Tek® [O.C.T. Compound, Sakura® Finetek], frozen in isopentane on dry ic,e and stored at -80°C for RNA extraction.

2.2. Animals

CH25H-deficient mice [*Ch25h*$^{-/-}$] in a C57BL/6 background were kindly provided by Novartis Institutes for BioMedical Research,[33] and bred in our animal facility with C57BL/6 mice to generate *Ch25h*$^{+/-}$ mice. *Ch25h*$^{+/-}$ were then crossed to obtain *Ch25h*$^{-/-}$ and *Ch25h*$^{+/+}$ [wild-type] littermates. The animals received standard laboratory mouse food and water *ad libitum*. They were housed under specific pathogen-free [SPF] conditions in individually ventilated cages; 7- to 10-week old female littermates were used for all studies.

2.3. DSS-induced chronic colitis

DSS-induced chronic colitis was induced by administration of four cycles of treatment with DSS [MP Biomedicals]. Every cycle consisted of 7 days of 2.5% DSS followed by 10 days of normal drinking water. Mice were killed 4 weeks after the last DSS cycle. The colon was fixed and embedded and cut transversally. Microscopy images were acquired from the last <1-cm parts of the colon, avoiding squamous cell epithelial sections [which are occasionally observed] and oblique sections. Colonoscopy was scored using the murine endoscopic index of colitis severity [MEICS] scoring system.[41] Histological scoring was performed on haematoxylin and eosin [HE]-stained distal colon sections, as described previously.[41,42] The investigator was blinded during image acquisition and scoring.

2.4. Heterotopic intestinal transplant model

The heterotopic mouse intestinal transplant model is an adaptation of the transplantation model of intestinal fibrosis in rats, which have both been described in detail previsously.[19,20] Briefly, donor small bowel was resected and transplanted subcutaneously into the neck of a recipient animal of the same gender and genotype. A single dose of cefazolin [Kefzol, 1 g diluted in 2.5 ml aqua dest.] was applied

intraperitoneally [i.p.] as infection prophylaxis. The time interval between graft resection and subsequent implantation was less than 15 min. No anaesthesia-related recipient death, post-transplantation recipient death, or evidence of infection was observed in any of the animals. Intestinal grafts were removed 7 days after transplantation. At explantation, each graft was divided into three equal segments. One segment was fixed in 4% formalin and prepared for histopathological assessment. The remaining segments were snap-frozen in liquid nitrogen and stored at -80°C for RNA extraction and hydroxyproline [HYP] assay, respectively.

For each sample, 10 mg of snap-frozen tissue was homogenised with 100 µl of ultrapure water in M tubes [Miltenyi Biotec], using a gentleMACS tissue homogeniser [Miltenyi Biotec]. Graft collagen content was evaluated using the HYP Assay Kit [Sigma-Aldrich] according to the manufacturer's instructions. HYP concentration is determined by the reaction of 4-[dimethylamino]benzaldehyde [DMAB] with oxidised HYP, resulting in a colourimetric product [560 nm], proportional to the presence of HYP. All samples and standards were run in duplicate, and absorbance at 560 nm was detected on a SpectraMax M2 fluorescence microplate reader using SoftMax Pro version 5 Software [Molecular Devices].

2.5. RNA isolation, cDNA synthesis, and real-time polymerase chain reaction

Total RNA was isolated using the RNeasy Plus Mini Kit [QIAGEN]. For mouse samples, lysis buffer from the kit was added to snap-frozen resections, and samples were shredded in M tubes [Miltenyi Biotec] in a gentleMACS tissue homogeniser [Miltenyi Biotec]. For human samples 10-µm thick tissue tek sections, containing the full thickness of the intestinal wall [confirmed by H/E staining], were cut using a cryostat. Sections were dissolved in TRIzol [Invitrogen, Life Technologies]. Total RNA was prepared according to the manufacturer's instructions. On-column DNase digestion with RDD buffer [QIAGEN] was performed for 15 min at room temperature. RNA concentration was determined by absorbance at 260 and 280 nm. Complementary DNA [cDNA] synthesis was performed using a High-Capacity cDNA Reverse Transcription Kit [Applied Biosystems] following the manufacturer's instructions. Real-time polymerase chain reaction [PCR] was performed using the TaqMan Fast Universal Master Mix [Applied Biosystems] on a Fast 7900HT Real-Time PCR System, and results analysed with the SDS software [Applied Biosystems]. The real-time PCR started with an initial enzyme activation step [5 min, 95°C], followed by 45 cycles consisting of a denaturing [95°C, 15 s] and an annealing/extending [60°C, 1 min] step. For each sample, triplicates were measured and glyceraldehyde-3-phosphate dehydrogenase [GAPDH] was used as endogenous control. Results were analysed by the ΔΔCT method. All gene expression assays were obtained from Life Technologies.

2.6. Analysis of microscopy images

Sections were examined using an AxioCam HRc [Zeiss] on a Zeiss Axio Imager.Z2 microscope with AxioVision release 4.8.2 software. Collagen layer thickness was measured on Sirius Red-stained slides in at least eight fields in representative areas at 100-fold magnification, by an investigator blinded to the experiment. The muscularis mucosae and the external muscle layer were quantified by a similar procedure, with an investigator blinded to the genotype of the animals. Great effort was made by the investigator and the advising gastrointestinal pathologist [SL] to restrict measurements to horizontally cut sections of the colon and also in colon sections in animals with DSS colitis [which typically leads to a disrupted crypt architecture]. For the automated microscopy analysis of DSS colitis, Sirius Red-stained slides were analysed by bright-field microscopy, and images were acquired by an investigator blinded to the genotype. The images were analysed using MATLAB software, version 8.6 R2015b [MathWorks]. Customised scripts identified the collagen layer of each image by clustering pixels of similar colours in five clusters, using the k-means clustering algorithm. Wild-type and knockout animals were used in the same batch with the same settings, to ensure an objective and unbiased analysis.

Microscopy images for the heterotopic transplant model were acquired and analysed in a similar manner, except that a polarising filter was used. Under polarised light, Sirius Red-stained collagen assumes a palette of colours ranging from green to red, based on the fibrotic maturation process. Our MATLAB scripts identified two cluster of pixels [collagen and non-collagen] using highly similar k-means clustering algorithms.

2.7. Western blot

Tissue was lysed in M-PER cell lysis buffer [Thermo Fisher Scientific]. Protein levels were determined by bicinchoninic acid [BCA] assay according to the manufacturer's instructions, and equal amounts of protein were loaded onto SDS/PAGE gels. Western blots were performed using monoclonal rabbit anti-mouse TGF-β antibodies [3711S, Bioconcept, 1:1000], polyclonal rabbit anti-mouse β-actin antibodies [4970, 13E5, Cell Signaling, 1:2000], polyclonal goat anti-mouse α-SMA antibodies [PA5-18292, Thermo Fisher Scientific, undiluted], and the horseradish peroxidase-conjugated secondary goat anti-rabbit antibody [sc-2004, Santa Cruz, 1:2000]. Luminescence of Western blots was quantified densitometrically with ImageJ software.

2.8. Mass cytometry analysis

Data were acquired on a CyTOF-2.1 mass cytometer [Fluidigm] with an acquisition flow rate of 0.03 ml/min. The following signal processing settings were used: default thresholding scheme, lower convolution threshold of 800 intensity units [IU], minimum event duration of eight pushes, maximum event duration of 100 pushes, noise reduction active. All samples were spiked with EQ four-element calibration beads during acquisition [Fluidigm; cat. no. 201078] and resulting FCS [Flow Cytometry Standard] files were normalised with the built-in normalisation algorithm [Helios software version 6.5.358] to account for intra- and intersample intensity measurement variability. The data were analysed and visualised with Cytobank software [Cytobank Inc.] and software packages for R programming language flowCore, flowSOM and ggplot2.

2.9. RNA *in situ* hybridisation [RNAscope]

Ch25h mRNA localisation in the murine small intestine was assessed by RNA *in situ* hybridisation. Fresh small intestine sections and intestine grafts were harvested and incubated for 24 h in 4% paraformaldehyde/PBS [PFA/PBS]. The PFA/PBS solution was replaced by 10% sucrose in PBS up to the tissue sink to the bottom of the container. This step was repeated with 20% and 30% sucrose solutions, and the tissue was embedded in Optimal Cutting Temperature [OCT]. Sections [3–4 µm] were prepared on Superfrost microscope slides [Thermo Fisher Scientific, Braunschweig, Germany]. The RNA *in situ* hybridisation was performed using the RNAscope 2.5 HD assay, Red [Advanced Cell Diagnostics, Hayward, CA, USA] following the manufacturer's instructions.

In brief, slides were rehydrated in PBS and were subjected to pretreatment solutions using the recommended incubation time and temperature. Next, slides were incubated for 2 h with a Ch25h probe designed and provided by the supplier. The tissue and assay quality were tested with a positive control probe Peptidyl-prolyl cis-trans isomerase B [Ppib, data not shown] and a negative control probe for the bacterial gene Dihydrodipicolinate reductase [Dapb]. Four signal amplification steps were carried out at 40°C, followed by two additional steps at room temperature with the appropriate solutions. The fifth amplification step was extended from 30 min to 1 h in order to enhance the chromogenic signal. Detection of chromogenic signals was achieved by using the Fast-Red reagent for 10 min. Slides were counterstained with haematoxylin I and mounted with VectaMount Mounting Medium HT-5000 [Vector Laboratories, Burlingame, CA, USA].

2.10. Immunohistochemistry

Three-µm consecutive section pairs of intestinal grafts were prepared for *in situ* hybridisation and immunohistochemistry. Sections used for immunohistochemistry were blocked with Avidin/Biotin blocking reagents [Avidin/Biotin blocking kit, Vector Laboratories, Burlingame, CA, USA], and with one drop of Bloxall [Vector Laboratories, Burlingame, CA, USA] as described by the manufacturer. After washing once with PBS for 5 min, sections were blocked with 2% BSA for 15 min and incubated with 1:400 rabbit anti-αSMA antibody [ab5694, Abcam, Cambridge, UK] overnight at 4 °C. Next, slides were washed twice with hypertonic PBS [18 g NaCl /L] for 5 min and sections were incubated at room temperature for 1 h with 1:500 secondary antibody Biotin-SP-conjugated donkey anti-rabbit IgG [H+L] [Jackson ImmunoResearch, West Grove, PA, USA]. Slides were washed twice in PBS, and the immunohistochemical staining was obtained by incubating graft sections for 40 min with Vecstatin Elite ABC reagent [Vector Laboratories, Burlingame, CA, USA]. ABC solution was washed twice with PBS and replaced by DAB solution for 1 min [prepared as described by the manufacturer: Vector Laboratories, Burlingame, CA, USA]. After washing for 5 min in water, sections were counterstained with haematoxylin [Hämalaun verstärkt nach Mayer, Artechemis AG, Zofingen, Switzerland] and Eosin Y [HT110132, Sigma-Aldrich, Steinheim, Germany], followed by dehydration in alcohol gradient [dipping in 70%, 96%, and 100% ethanol]. Mounting was performed as described for *in situ* hybridisation.

2.11. *In vitro* experiments

3T3 cells were maintained in high glucose Dulbecco's Modified Eagle Medium [DMEM, Life Technologies] supplemented with 10% fetal calf serum [FCS] and kept at 37°C in a humidified atmosphere containing 5% CO_2. Murine primary fibroblasts were isolated and cultured as described previously.[43] The isolated cells were cultured in 25-cm^2 culture flasks [Costar, Bodenheim, Germany] with DMEM containing 10% FCS, penicillin [100 IE/mL], streptomycin [100 g/mL], ciprofloxacin [8 g/mL], gentamycin [50 g/mL], and amphotericin B [1 g/mL] at 37°C in a humidified atmosphere containing 10% CO_2. Non-adherent cells were removed. Once fibroblasts reached 90% confluence, FCS-free DMEM-medium was added and they were starved for 24 h before compound treatment. Cells were stimulated by treatment for 72 h with 5 ng/ml TGF-β [130-095-067, Miltenyi Biotec], 0.001–10 µM 25-HC [H1015, Sigma-Aldrich], or a combination of the two compounds as indicated.

2.12. Statistical analysis

Data are presented as mean ± standard error of the mean [SEM] unless otherwise indicated. Correlation was assessed using non-parametric Spearman rank analysis. Significance of group-wise comparisons was assessed using the Kruskal-Wallis test, Mann-Whitney U test or the unpaired t test with $p < 0.05$ considered statistically significant [$^{***}p < 0.001$, $^{**}p < 0.01$, $^{*}p < 0.05$].

2.13. Study approval

For patient data, written informed consent was obtained for anonymous use of patient data and resected parts of human intestine according to the code of conduct for responsible use of surgical rest material (Research Code University Medical Center Groningen [http://www.rug.nl/umcg/research/documents/ research-code-info-umcg-nl.pdf, see Code goed gebruik voor gecodeerd lichaamsmateriaal]). Mouse experiments were approved by the local animal welfare authority [Tierschutzkommision Zürich, Zurich, Switzerland; registration number ZH183/2014].

3. Results

3.1. *CH25H* mRNA expression is a marker of fibrosis in intestinal samples of CD patients

To test for a role of the oxysterol synthesising enzyme CH25H in CD associated fibrosis, *CH25H* mRNA expression was measured in

Table 1. Characteristics of patients with CD and controls.

	Crohn's disease [n = 7]	Control [n = 6]
General		
Gender, *n* [%] female	7 [100%]	5 [83%]
Age at sample, years [mean, min-max]	36[26–65]	72.7[67–82]
Disease duration, years, [mean, min-max]	9.6[1–35]	NA
Montreal age at diagnosis, *n* [%]		
17–40 years [A2]	7 [100%]	NA
Montreal disease behaviour, *n* [%]		
Stricturing disease [B2]	7 [100%]	NA
Disease location, *n* [%]		
Terminal ileum [L1]	4 [57%]	NA
Ileocolon [L3]	3 [43%]	
C-reactive protein before operation, *n* [%]		
C-reactive protein >5 mg/L	2 [28%]	NA
C-reactive protein <5 mg/L	3 [43%]	
Missing	2 [29%]	
Clinical disease activity before operation, *n* [%]		
Disease in remission	0 [0%]	NA
Mild disease	1 [14%]	
Moderate disease	3 [43%]	
Severe disease	3 [43%]	
Medication, *n* [%]		
Corticosteroids	4 [57%]	
Azathioprine/6-mercaptopurine	3 [43%]	NA
Anti-TNF	0 [0%]	
Anti-IL12/23	1 [14%]	

NA, non-applicable; CD, Crohn's disease; min-max, minimum to maximum; TNF, tumour necrosis factor.

human intestinal surgical samples. We investigated terminal ileum samples from CD patients undergoing ileocaecal resection due to stenosis. Samples macroscopically affected by fibrosis were compared with the proximal ileal resection margin which showed no macroscopic signs of fibrosis or inflammation. Healthy tissue, from cancer-free resection margins of colon adenocarcinoma patients undergoing right-sided hemicolectomy, was used as additional control [Table 1]. Representative Sirius Red-staining pictures illustrate increased collagen deposition in fibrotic areas of CD patients [Figure 1A]. We observed a gradual increase of *CH25H* mRNA expression from control tissue to non-fibrotic CD tissue and to fibrotic areas from the same patients [p <0.05, Figure 1B]. Thereby, mRNA levels of *CH25H* strongly correlated with the expression levels of fibrosis markers including *COL-1* and *-3*, *SMA*, and *TGF-β* [Figure 1C–F], confirming the association of CH25H expression with intestinal fibrosis in the human intestine.

Of note, control patients were older than patients with CD with or without fibrosis. This is expected since the incidence of CD peaks at a younger age than colorectal carcinoma, and elderly CD patients are at lower risk for strictures than younger individuals.[44,45] However, it is unlikely to explain the observed difference in *CH25H* expression, since regulation of CH25H does not depend on age.[46]

3.2. Reduced intestinal fibrosis in mice with deficient 25-hydroxycholesterol synthesis

To further investigate the role of CH25H in intestinal fibrosis, we investigated whether absence of CH25H would reduce fibrosis in dextran sodium sulphate [DSS]-induced chronic colitis, a well-established model of intestinal inflammation, typically associated with high levels of intestinal fibrosis.[17,18] For this aim, we induced chronic colon inflammation and fibrosis in wild-type [WT] and *Ch25h*$^{-/-}$ littermate mice, with four cycles of 7 days 2.5% DSS in drinking water followed by a 10-day recovery period with normal drinking water. Collagen deposition was determined by Sirius Red staining and analysis under transmission light microscopy [Figure 2A]. Reduced collagen deposition in *Ch25h* knockout mice was demonstrated by automated quantification of the collagen layer area [Figure 2B, C]. Further, the collagen layer was significantly thinner in DSS-treated *Ch25h*$^{-/-}$ mice compared with WT littermate DSS-treated animals: WT: 22.4 µm ± 7.2, *Ch25h*$^{-/-}$: 11.7 µm ± 2.6, p = 0.008]. In water controls, in the absence of inflammation, the baseline collagen layer is indistinguishable from wild-type animals [Figure 2D, water animals: WT: 8.5 µm ± 2.1, *Ch25h*$^{-/-}$: 8.7 µm ± 0.8, p = 0.17]. Microscopy analysis and histological scoring of inflammation [see below] did not reveal any differences between non-inflamed wild-type and *Ch25h*$^{-/-}$ animals.

Additionally, mRNA expression levels for fibrosis markers such as *Tgf-β*, collagen type 3 [*Col-3*] and *Timp-1* were significantly lower in the colon of *Ch25h*$^{-/-}$ animals, and a clear trend for lower mRNA expression of collagen type 1 *[Col-1*] and lysyl oxidase homologue 2 [*Loxl-2*] in CH25H-deficient mice was found [Figure 2E–J]. Immunohistochemistry demonstrated high α-SMA expression in fibrotic sections of wild-type animals and reduced α-SMA expression in CH25H-deficient mice [Supplementary Figure S1, available as Supplementary data at *ECCO-JCC* online]. Expression levels of *Ch25h* were increased in DSS-treated animals compared with water controls [Figure 2J].

Of note, thinner collagen layers and lower expression levels of fibrosis markers [*Tgf-β*, *Col-3*, and *Timp-1]* upon *Ch25h* knockout were

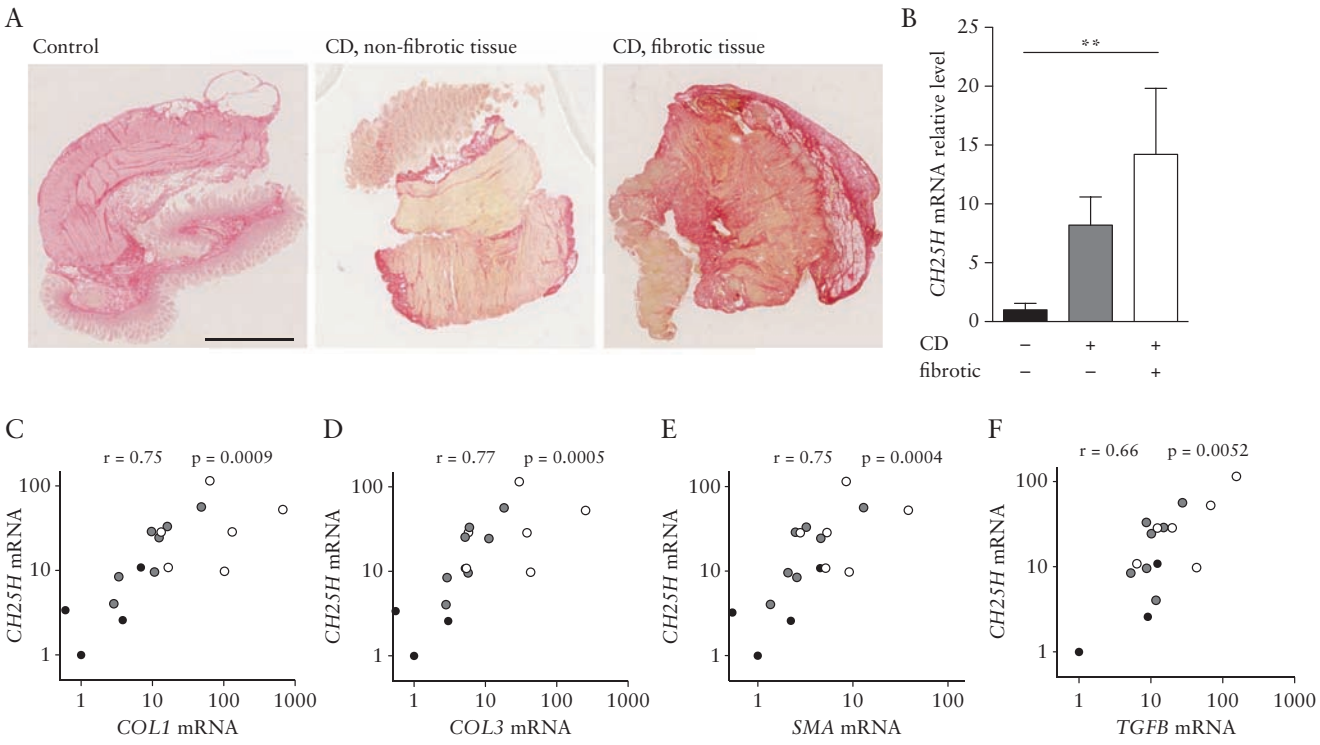

Figure 1. Upregulation of *CH25H* mRNA expression in human fibrotic tissue of patients with CD. [A] Representative images of Sirius Red-stained human ileum samples from healthy controls [left panel] and CD patients in a non-fibrotic [middle panel] and in a fibrotic region [right panel]. Scale bar: 2.5 mm. White: CD fibrotic, [n = 6], grey: CD non-fibrotic [n = 7], black: healthy control [n = 6]. [B] Samples were analysed for *CH25H* mRNA expression and normalised to *GAPDH*. *CH25H* mRNA level was correlated with mRNA levels of [C] *Col1*, [D] *Col3* [E] *SMA*, and [F] *TGFB*. Statistical analysis: B: Kruskal-Wallis test; **p <0.01. CD, Crohn's disease. C-E: correlation analysis: Spearman R [non-parametric correlation].

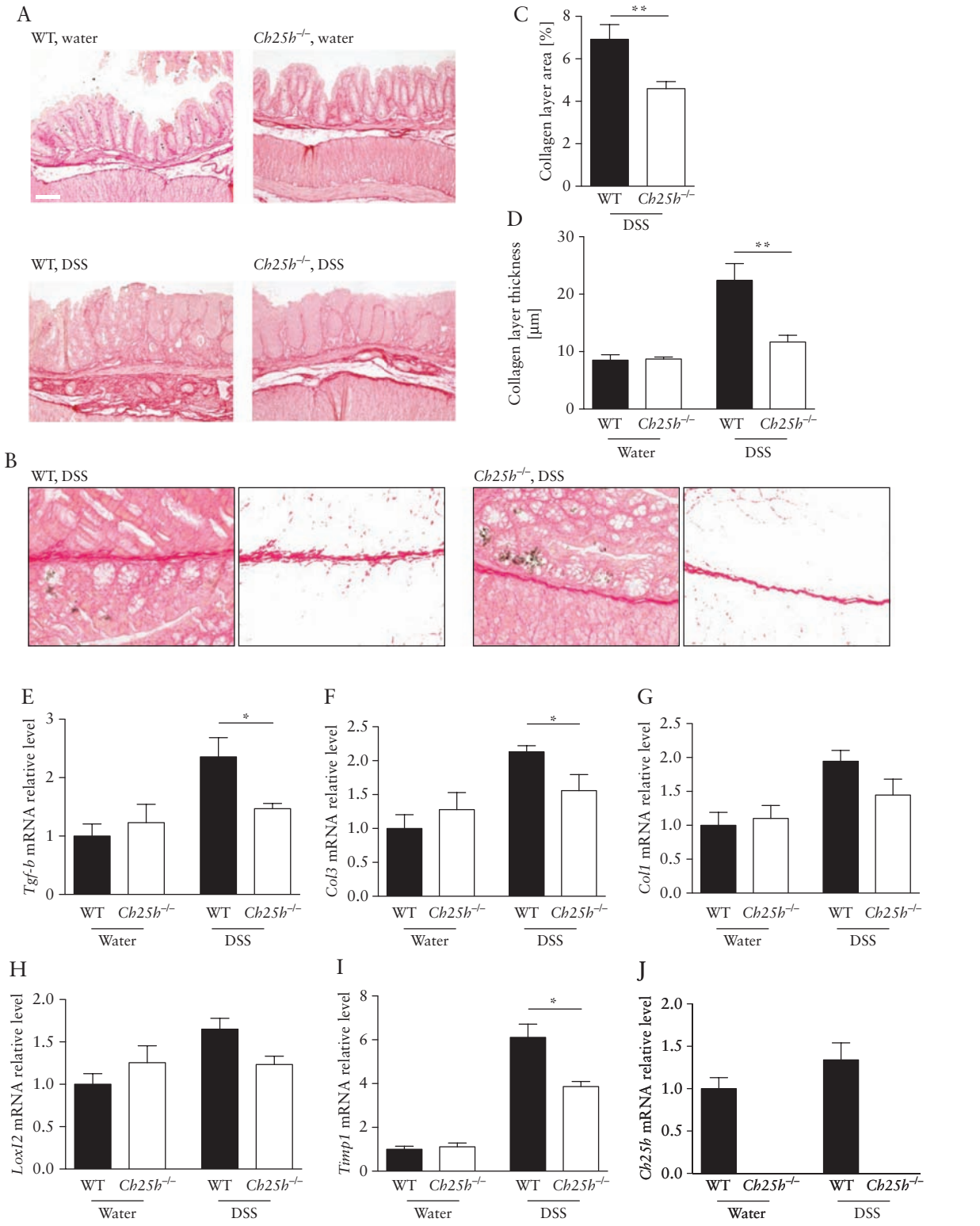

Figure 2. Reduced fibrosis in *Ch25h*$^{-/-}$ mice in chronic DSS colitis. *Ch25h*$^{-/-}$ and WT female mice were treated for four cycles with 2.5% DSS or water [controls]. [A] Representative transmission light images of Sirius Red-stained intestinal sections of wild-type [WT] and *Ch25h*$^{-/-}$ dextran sodium sulphate [DSS]-treated mice and water littermate controls. Scale bar: 100 µm. [B] Image analysis for identification of collagen layer areas in the colon mucosa using Matlab custom-made scripts. Left panel: Original transmission light Sirius Red-stained image. Right panel: Collagen layer area. [C] Quantification of collagen layer area in DSS-treated animals using customised Matlab scripts. [D] Collagen layer thickness calculated from eight or more positions per graft in representative areas of Sirius Red-stained slides with transmission light at 200-fold magnification. The colon was analysed for mRNA expression of: [E] *Tgf-beta*, [F] *Col3*, [G] *Col1*, [H] *Loxl2*, [I] *Timp1*, and [J] *Ch25h* [normalised to *Gapdh*]. Expression levels are normalised to water-treated wild-type controls. Statistical analysis: Mann-Whitney U test; *p <0.05. n = 4–6 per group.

not due to reduced inflammation: when colon inflammation was analysed in H/E stained colon sections, the histology score quantifying the inflammatory infiltrate and the epithelial damage, was even higher in *Ch25h*$^{-/-}$ mice compared with WT littermates [Figure 3A]. Further, macroscopic aspects of intestinal inflammation, such as spleen weight and the murine endoscopic index of colitis severity [MEICS], did not differ between both genotypes [Figure 3B], with similar thickening of the colonic surface (2.30 points ± 0.57 [n = 6] vs 2.25 points ± 0.82 [n = 5], p >0.05, Supplementary Figure S2A, B, available as Supplementary data at *ECCO-JCC* online). Detailed measurements of the muscularis mucosae and external muscle layer did not yield significant differences between genotypes [Supplementary Figure S2C–E, available as Supplementary data at *ECCO-JCC* online]. In summary, in chronic DSS colitis, intestinal collagen deposition was reduced in the absence of CH25H, independently of effects of CH25H knockout on intestinal inflammation.

3.3. Reduced intestinal fibrosis in the absence of CH25H in a heterotopic transplant model of intestinal fibrosis

To confirm a role of CH25H in intestinal fibrosis in an inflammation-independent model, we employed a recently developed heterotopic transplant model of intestinal fibrosis.[19,20] Sections of small intestine, from either CH25H knockout [*Ch25h*$^{-/-}$] mice or their wild-type littermate controls [WT], were transplanted subcutaneously into the neck of recipient mice of the same genotype.[19,20] Non-transplanted small bowel sections from *Ch25h*$^{-/-}$ mice and WT littermates were used as controls [Day 0]. Seven days after surgery, the intestinal grafts were collected for analysis [Day 7] and collagen deposition was determined by Sirius Red staining under transmission light microscopy. At baseline [Day 0], cross sections of WT and *Ch25h*$^{-/-}$ were histologically indistinguishable, with intact epithelial crypts and a thin collagen layer. Seven days following transplantation, occlusion of the intestinal lumen and a significantly thicker collagen layer were observed [Figure 4A, overview]. We also confirmed partial destruction of the intestinal epithelial layer with loss of epithelial cells 7 days after transplantation [Figure 4A, detail] compared with freshly isolated tissue on Day 0 [Figure 4A, detail], as expected for this model.[19,20]

The development of intestinal fibrosis was significantly reduced in mice deficient for CH25H, indicated by a significantly thinner collagen layer compared with WT littermate controls (Figure 4A, B; Day 0: WT: 8.5 µm ± 0.7, *Ch25h*$^{-/-}$: 8.3 µm ± 1.5 non-significant [n.s.], Day 7: WT 15.0 µm ± 3.1, *Ch25h*$^{-/-}$: 12.1 µm ± 2.3, p = 0.01). A thinner collagen deposition in *Ch25h* knockout mice was confirmed by polarised light microscopy with automated image analysis and quantification of the collagen layer area [Figure 4C, D]. Furthermore, concentration of the collagen metabolite

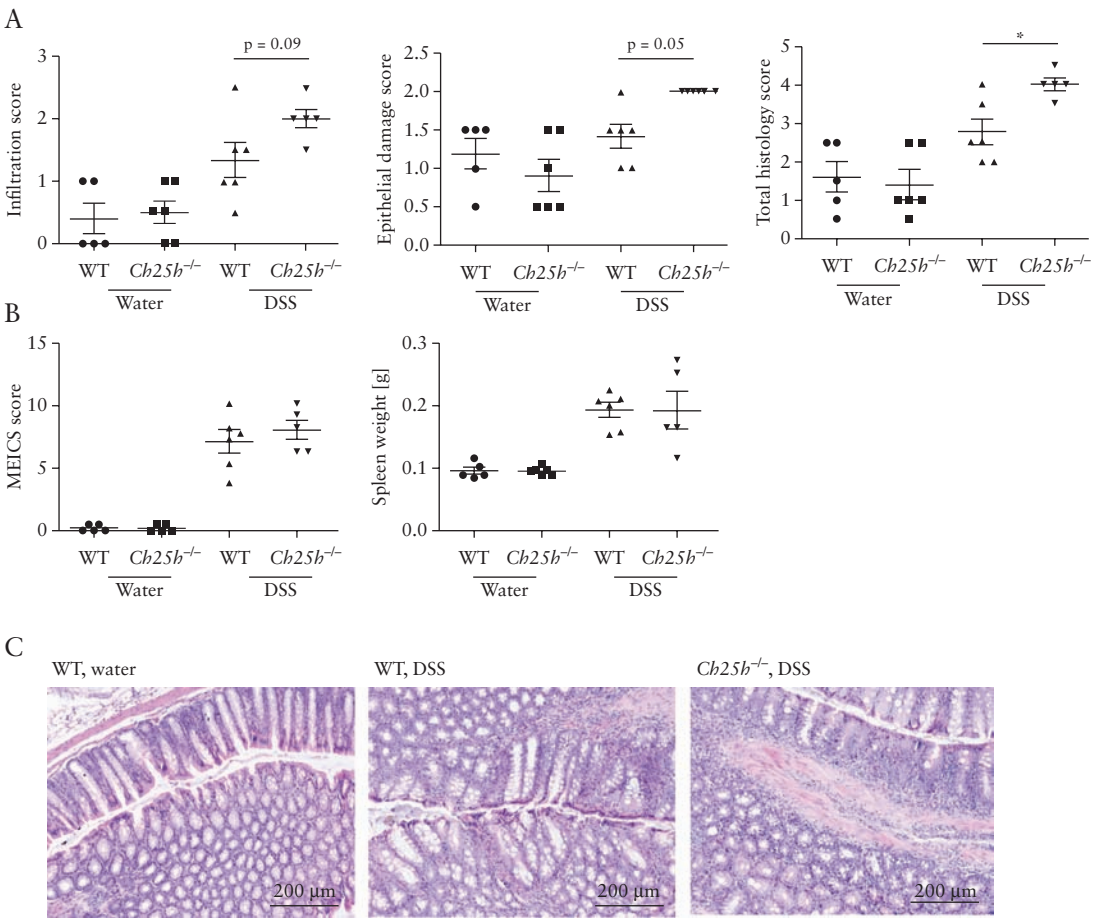

Figure 3. Reduced levels of intestinal fibrosis in CH25H-deficient mice is not due to reduced inflammation in chronic DSS colitis. Analysis of colon inflammation in H/E-stained colon sections. [A] Score of the inflammatory infiltrate [left panel], score for epithelial damage [middle panel], and total histology score [sum of both partial scores, right panel]. [B] Murine endoscopic index of colitis severity [MEICS] score [left panel] and spleen weight [right panel]. [C] Representative H/E-stained sections of the distal colon of water control mice [left panel] and DSS-treated mice. DSS, dextran sodium sulphate; H/E: haematoxylin and eosin.

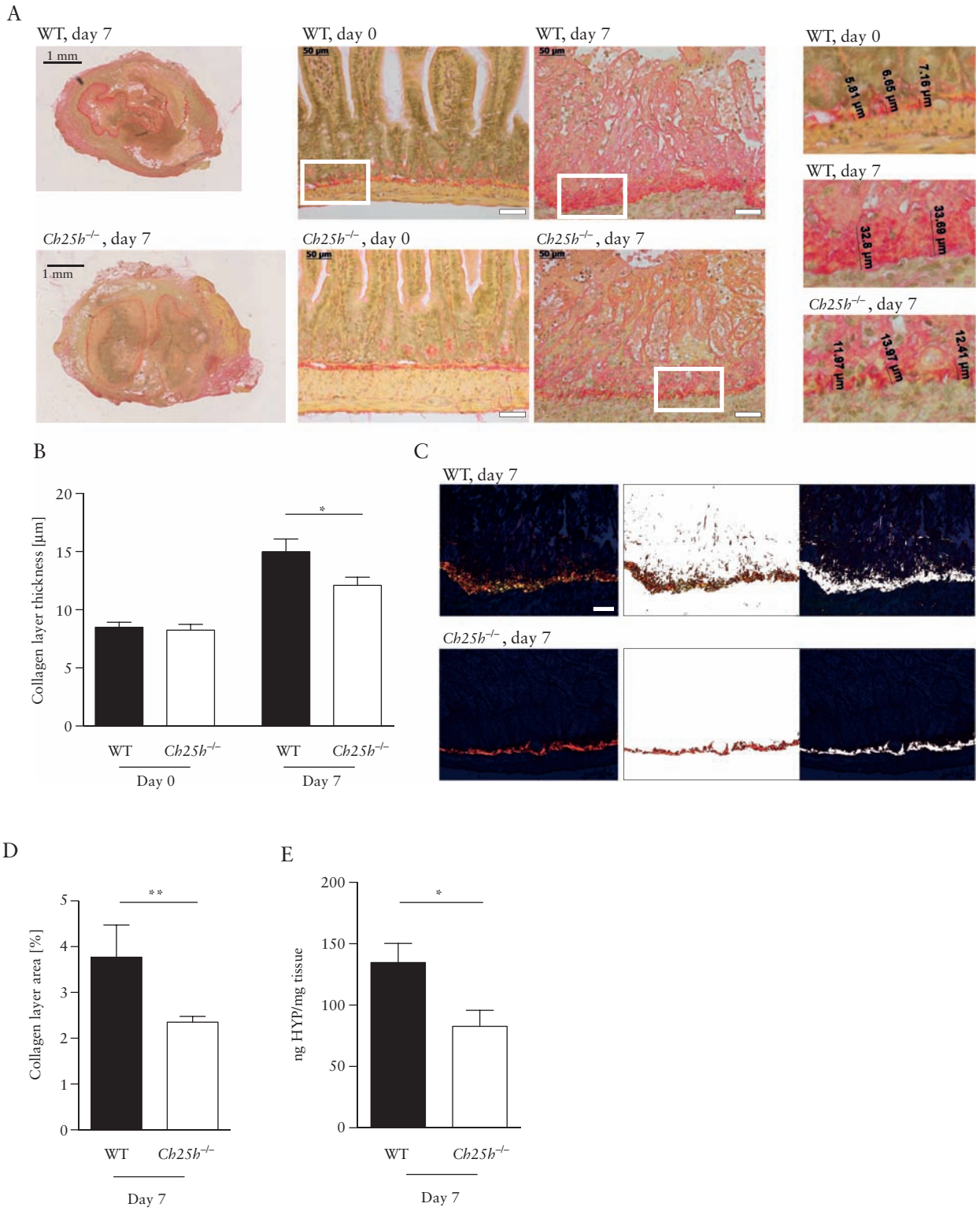

Figure 4. Reduced levels of intestinal fibrosis in CH25H-deficient mice in the heterotopic transplantation model. Wild-type and *Ch25h*$^{-/-}$ animals were tested in a heterotopic transplantation model for intestinal fibrosis. [A] Left panels: Overview [low-resolution image] of Sirius Red-stained intestinal grafts of WT and *Ch25h*$^{-/-}$ mice at Day 7 after transplantation. Scale bar: 1 mm. Middle panels: Representative transmission light images demonstrating increased collagen layer thickness in grafts at Day 7 compared with freshly isolated intestines at Day 0. Upper panels: WT littermate controls. Lower panels: *Ch25h*$^{-/-}$. Scale bar: 50 µm. Right panels: High-resolution inserts illustrating measurements of collagen layer thickness. [B] Collagen layer thickness calculated from eight or more positions per graft in representative areas of Sirius Red-stained slides with transmission light at 200-fold magnification. [C] Image analysis for identification of collagen layer areas using Matlab custom-made scripts. Left panel: Original polarised 200x light microscopy image. Middle panel: Collagen layer area. Right panel: Remaining non-collagen tissue. Scale bar: 50 µm. [D] Quantification of collagen layer area at Day 7 post transplantation, using the same strategy as in [C]. [E] Collagen quantification with hydroxyproline assay. Day 0, freshly isolated intestine. Day 7, intestine 7 days post transplantation [n_{WT} day 0 = 3, n_{KO} day 0 = 9, n_{WT} day 7 = 8, n_{WT} day 7 = 11]. Statistical analysis: Mann-Whitney U test; *p <0.05, **p <0.01. Bars indicate mean ± standard error of the mean [SEM]. WT, wild type; CH25H, cholesterol 25 hydroxylase; HYP, hydroxyproline.

hydroxyproline was significantly lower in *Ch25h* knockout intestinal transplants compared with WT littermate controls [Figure 4E].

Ch25h mRNA expression was significantly increased in fibrotic small bowel resections 7 days after transplantation compared with freshly isolated intestine [Figure 5A]. Similarly, fibrosis markers including *Col-1*, *Mmp-9*, and *Timp-1* were induced 7 days after transplantation compared with Day 0 [Figure 5B–D]. *Ch25h*$^{-/-}$ animals displayed a non-significant trend for reduced expression of fibrosis markers compared with WT controls at Day 7 [Figure 5B–D]. TGF-β protein levels were decreased in *Ch25h* knockout as compared with WT mice, in line with reduced stimulation of profibrotic pathways upon CH25H deficiency [Figure 5E, F]. Thus, in agreement with the DSS-induced chronic colitis model, our heterotopic transplant model confirms reduced intestinal fibrosis in the absence of CH25H.

3.4. Recruitment of immune cells into fibrotic small intestine in wild-type and *Ch25h*$^{-/-}$ animals

To address changes in immune cells infiltrating the intestinal grafts, lamina propria mononuclear cells were isolated from the grafts

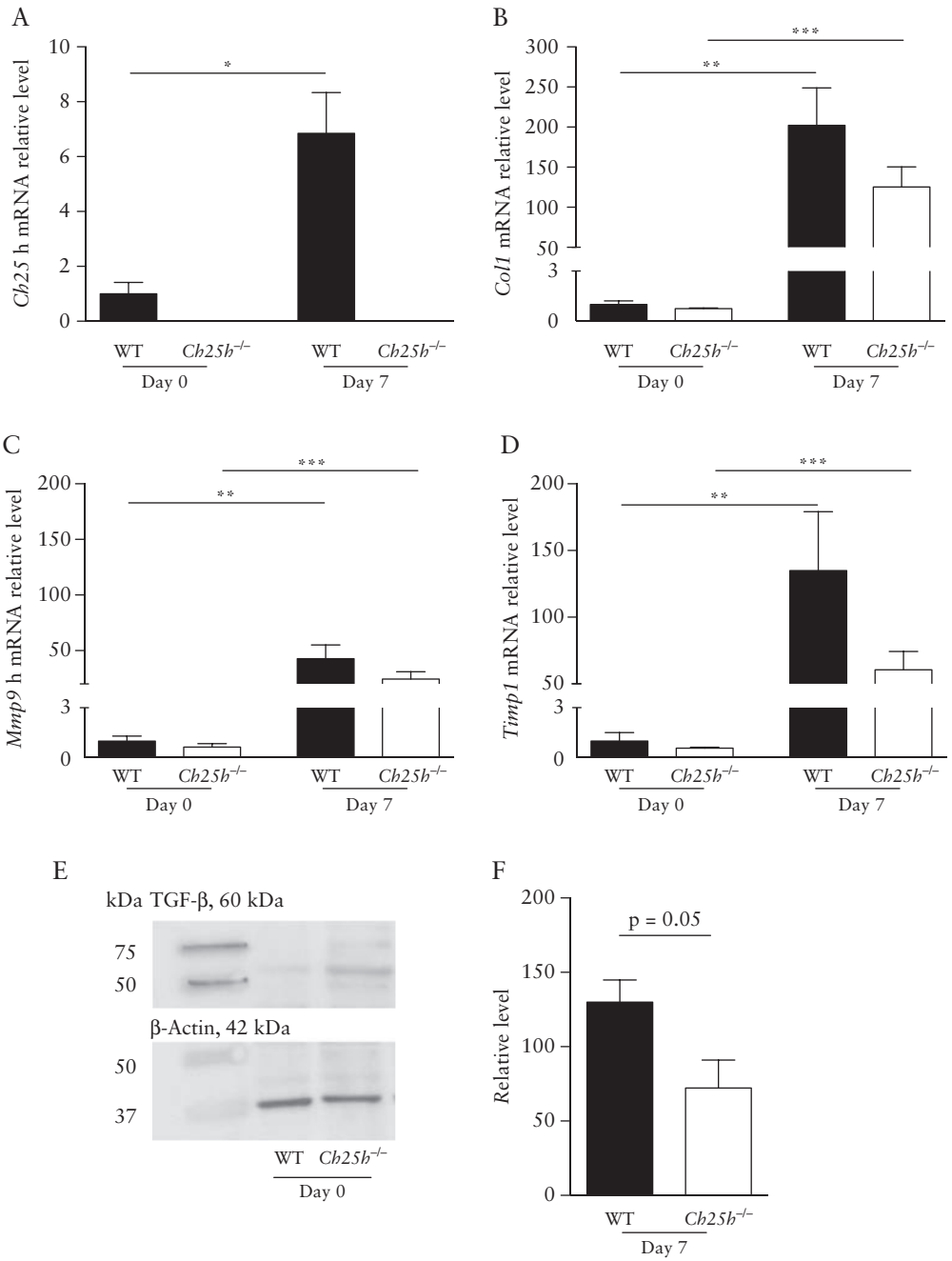

Figure 5. Expression of intestinal fibrosis markers in wild-type and *Ch25h*$^{-/-}$ mice. Wild-type and *Ch25h*$^{-/-}$ mice were tested in a heterotopic intestinal transplant model. Freshly isolated intestines [Day 0] and grafts 7 days after transplantation were analysed for mRNA expression of: [A] *Ch25h*, [B] *Col1*, [C] *Mmp9*, and [D] *Timp1* [normalised to *Gapdh*]. [E, F] Analysis of protein expression of TGF-β by Western blot. Statistical analysis: A-D: Mann-Whitney U test; $*p < 0.05$, $**p < 0.01$ [n_{WT} day 0 = 3, n_{KO} day 0 = 9, n_{WT} day 7 = 8, n_{WT} day 7 = 11]. E-F: $n = 4$. Unpaired t test.

7 days after surgery and an explorative mass cytometry [Cytometry by Time of Flight, CyTOF] analysis with a broad marker panel [Table 2] was performed. Cells were automatically clustered based on similarity of surface marker expression. The immune cell infiltrate was dominated by neutrophils, with a lower fraction of T cells, dendritic cells, monocytes, and NK cells [Figure 6A, B]. No significant differences between WT and *Ch25h*$^{-/-}$ animals were detected for the investigated immune cell populations [Figure 6C]. Additionally, histological analysis of IL-17 revealed no differences in IL-17 expression between WT and *Ch25h*$^{-/-}$ grafts [Supplementary Figure S3, available as Supplementary data at *ECCO-JCC* online].

To determine the location of *Ch25h* mRNA expression in the small intestine, RNA *in situ* hybridisation using fixed-frozen sections of intestinal grafts and freshly isolated intestines was performed. *Ch25h* mRNA expression was detected in freshly isolated intestines from WT mice and the graft at 7 days after transplantation [Figure 7A, B, Supplementary Figure S4, available as Supplementary data at *ECCO-JCC* online].

The *Ch25h* signal appears to be cytoplasmic with the formation of small clusters. *Ch25h* expression was observed in fibroblasts demarcating the necrotic former mucosa layer, but remains of epithelial crypts were not found in the demarcation zone. The *Ch25h*-expressing, spindle-shaped fibroblasts are arranged in a band-like fascicle with large ovoid nuclei exhibiting a thinly dispersed chromatin structure and a delicate nuclear membrane without the indentations typically found in the nuclei of histiocytes [Figure 7B, arrows]. In contrast, *Ch25h* is not expressed in the inflammatory infiltrate, which mainly consists of neutrophils showing characteristic segmented nuclei [Figure 7B, double arrows]. No *Ch25h*-expressing lymphocytes were found. When both *Ch25h* expression and a-SMA were simultaneously assessed, significant co-localisation of both markers was found, in line with a fibroblast origin of *Ch25h*-expressing cells [Figure 7C].

3.5. 25-HC does not induce myofibroblast differentiation *in vitro*

To address direct effects of the CH25H product 25-HC on fibroblasts, we performed cell culture experiments using primary murine intestinal fibroblasts using a protocol similar to a previous study in a human lung fetal fibroblast cell line [HFL-1] .[39] Addition of TGF-β resulted in increased α-SMA protein expression in intestinal fibroblasts. In contrast, exposure to 25-HC did not affect α-SMA expression at 25-HC concentrations of 0.001–0.1 μM [Figure 7D], a concentration range covering values determined in human plasma before and after LPS exposure [0.01–0.025 μM] .[34] When higher oxysterol concentrations of 1–10 μM were tested, expression of the housekeeping gene β-actin was affected [Figure 7D]; results at such a high concentration range should be interpreted very cautiously.[47] Similarly, addition of 25-HC to 3T3 cells did not cause a significant increase of α-SMA expression at concentrations of 0.001–0.1 μM [Figure 7D].

Table 2. Antibodies used for CyTOF analysis.

Name	Clone	Reactivity	Tag
Ly6G	1A8	Mouse	141Pr
CD11c	N418	Mouse	142Nd
CD115	AFS98	Mouse	144Nd
CD69	H1.2F3	Mouse	145Nd
CD45	30-F11	Mouse	147Sm
CD11b [MAC1]	M1/70	Mouse	148Nd
CD19	6D5	Mouse	149Sm
Ly6C	HK1.4	Mouse	150Nd
CD25	3C7	Mouse	151Eu
CD3e	145-2C11	Mouse	152Sm
CD335, NKp46	29A1.4	Mouse	153Eu
CD62L	MEL-14	Mouse	160Gd
CCR7	4B12	Mouse	163Dy
CD8a	53–6.7	Mouse	168Er
TCRβ	H57-597	Mouse	169Tm
NK1.1	PK136	Mouse	170Er
CD44	IM7	Mouse, human	171Yb
CD4	RM4-5	Mouse	172Yb
I-A/I-E	M5/144	Mouse	174Yb
B220	RA3-6B2	Mouse	176Yb

All antibodies were pre-labelled [Fluidigm].

4. Discussion

In this study, we demonstrate a role of the oxysterol synthesising enzyme CH25H in the pathogenesis of intestinal fibrosis. mRNA expression of *CH25H* was upregulated in human intestinal fibrotic tissue of CD patients compared with healthy controls, and we found a positive correlation between expression of various fibrosis mediators and *CH25H* expression. Further, we demonstrate a contribution of CH25H to the development of intestinal fibrosis in two murine fibrosis models: in the DSS-induced colitis model, which is commonly used as a model of chronic intestinal inflammation and fibrosis,[17,18] mice lacking the CH25H enzyme showed less collagen deposition and lower mRNA levels of fibrosis mediators. In the recently developed heterotopic transplantation model, lack of CH25H also reduced intestinal collagen deposition as well as levels of the collagen metabolite HYP and the crucial pro-fibrotic factor TGF-β.[48,49] The HYP assay is not available for the chronic DSS colitis model, which is a limitation of our study.

In several aspects, the newly developed heterotopic transplantation model complements the DSS-induced model. The DSS-induced fibrosis model is well-established[50] and chronic DSS colitis, with cycles of DSS exposure and recovery, reflects many aspects of human CD with episodes of inflammation and recovery, leading to tissue remodelling and fibrosis. In DSS colitis, fibrosis is induced by disruption of the integrity of the mucosal barrier, resulting in bacterial translocation and lymphocyte infiltration, which promotes chronic colon inflammation. In this model, fibrosis has been assessed by microscopic imaging of collagen staining in the mucosa and submucosa, measurements of collagen metabolites [hydroxyproline assay], and magnetic resonance imaging [MRI] relaxometry.[51–53] Induction of fibrosis upon DSS exposure might depend on the mouse genotype[51] and can be observed after a single cycle of DSS treatment,[51,53] even though fibrosis further increases following 2 weeks of recovery and repeated DSS exposure.[52] The 2,4,6,-trinitrobenzene sulphonic acid [TNBS]-induced colitis is a colitis model that might better resemble human CD regarding transmural inflammation and induction of the adaptive immune response,[54] but is associated with other inherent limitations.[55]

In the heterotopic transplantation model, fibrosis is reliably induced within 7 days after transplantation. In contrast to DSS colitis, features of the transplantation model include occlusion of the lumen [reminiscent of human intestinal stenosis] and fibrosis of the small intestine, the organ most frequently involved in human CD. This new model also reflects other important aspects of the human disease, such as activation of intestinal myofibroblasts, expression of IL-13, TGF-β and α-SMA, and collagen deposition in the extracellular matrix.[20] In the transplantation model, fibrosis is associated with

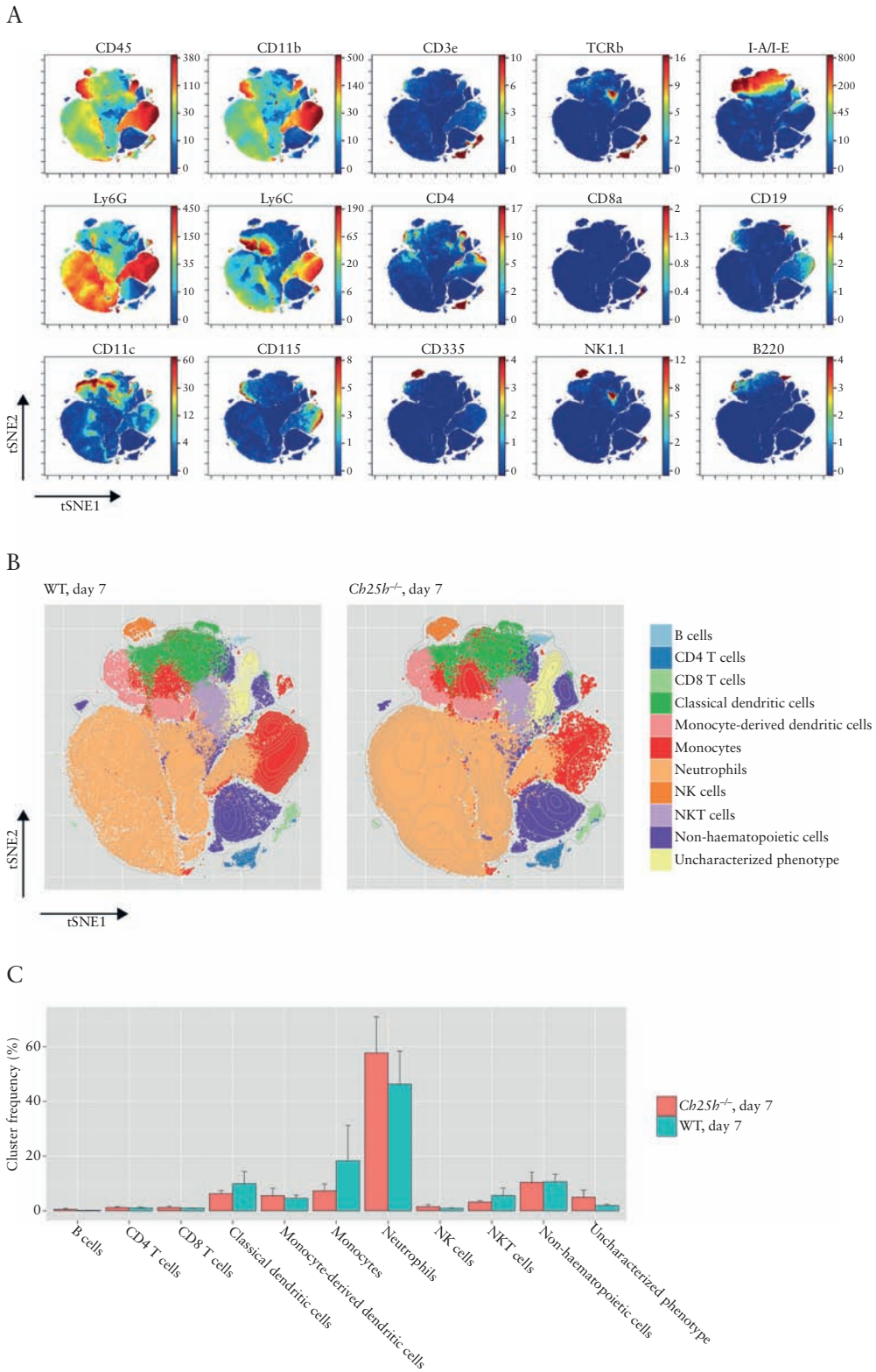

Figure 6. Cells infiltrating the graft do not differ between wild-type and CH25H-deficient mice. Lamina propria infiltrating cells from grafts of wild-type and Ch25h$^{-/-}$ mice were harvested 7 days after surgery and analysed by CyTOF. [A] Dimensionality-reduced projection of the entire phenotypical landscape was calculated using the tSNE algorithm with Barnes-Hut approximation [bhSNE]. The colour coding represents staining intensity of the specified marker. [B] t-SNE maps of each experimental group; 250 000 randomly selected points are plotted. Overlaid in colour are cluster designations computed by the Phenograph clustering algorithm. The represented clusters were manually constructed by merging the initial cluster output based on phenotypical similarity until the final number of 11 identifiable clusters was reached. [C] Bar plot showing the mean cluster frequencies and error bars representing standard error of the mean [SEM] [nWT = 5, nKO = 5].

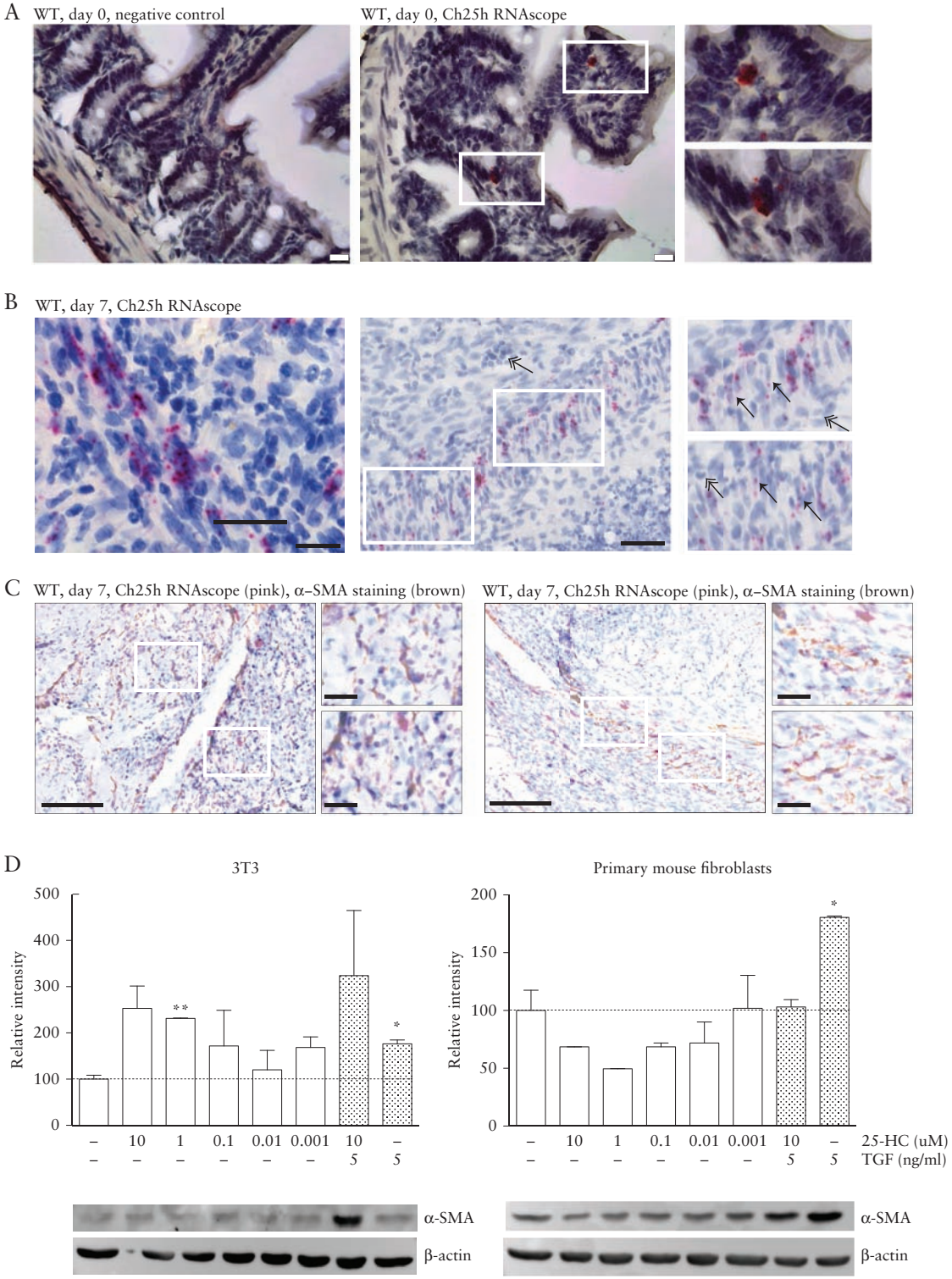

Figure 7. Expression of Ch25h in fibroblasts in intestinal grafts. [A] Representative images of the *in situ* hybridisation [RNAscope] analysis of wild-type small intestine. Negative control [a probe for the bacterial gene dihydrodipicolinate reductase, *Dapb*, left panel] and *Ch25h* mRNA [middle panel] are demonstrated with the RNAscope signal shown in red. Right panel: High resolution of inserts of the RNAscope signal. Scale bar: 25 μm. [B] Representative images of the *Ch25h* RNAscope analysis of the intestinal grafts of wild-type [WT] mice at Day 7 after transplantation, demonstrating accumulation of the CH25H signal in fibroblasts in the former mucosa layer. Scale bar left panel: 20 μm, middle panel: 50 μm. The right panel shows inserts of the middle panel. Fibroblasts are indicated by arrows, neutrophils by a double arrow. [C] Overlay of *Ch25h* RNAscope analysis and the α-SMA staining from two representative images with enlarged inserts. Scale bar: 100 μm, scale bar insert: 20 μm. [D] 3T3 cells [left panel] and primary mouse intestinal fibroblasts [right panel] were treated for 72 h with different concentrations of 25-HC and/or TGF-β as indicated. Samples were analysed for α-SMA protein levels by Western blot. Expression levels are normalised relative to the negative control and shown as mean ± standard error of the mean [SEM]. Statistical analysis: unpaired t test, the * is relative to the negative control; $*p < 0.05$, $**p < 0.01$, $n = 2$.

ischaemia and hypoxia, increased expression of *Hif1α*, and neovascularisation. However, bacterial translocation and the pathogen associated molecular pattern [PAMP]-associated signalling is not a prerequisite of fibrosis in this model, as collagen deposition is also increased following transplantation of small bowel from germ-free mice and MyD88-deficient mice.[56] In the heterotopic transplant model, fibrosis is also observed in the absence of B and T cells in RAG2-deficient mice [M. Hausmann, unpublished observations].

There is general consensus that currently there is no animal model available which would reflect all aspects of human CD-associated intestinal fibrosis.[50,54,55] However, in DSS colitis and small intestinal heterotopic transplantation, complementary clinical features can be studied and fibrosis seems to be induced by different pathways. Robust reduction of fibrosis upon CH25H knockout in two independent fibrosis models clearly strengthens the validity of our findings.

Our data demonstrate *Ch25h* expression in local fibroblasts in intestinal grafts, which potentially leads to local 25-HC production by fibroblasts. However, it remains unclear which cell[s] respond to 25-HC during fibrosis induction. In a previous *in vitro* study, 25-HC induced nuclear factor-κB [NF-κB] activation and subsequent release of TGF-β in human fetal lung fibroblasts, ultimately leading to α-SMA expression and myofibroblast differentiation.[39] In support of this finding, activation of NF-κB by 25-HC was also demonstrated in primary rat hepatocytes and in a human monocytic cell line.[57,58] However in our study, addition of 25-HC to 3T3 fibroblasts or primary murine intestinal fibroblasts failed to induce α-SMA expression. Therefore in the intestine, cells different from fibroblasts might be responsible for TGF-β production upon 25-HC exposure.

Previous reports demonstrated that 25-HC inhibits Th17 cell differentiation,[24,59] and *Ch25h* knockout mice have higher numbers of Th17 cells in peripheral lymph nodes and the spleen.[60] Th17-derived IL-17 is a key driver of fibrosis in different organs, including the gut.[61–63] However, histological analysis and quantification of IL-17 revealed no differences between WT and *Ch25h*$^{-/-}$ intestinal grafts. Further, our histological analysis revealed no decrease in intestinal inflammation between wild-type and *Ch25h*$^{-/-}$ littermate controls in chronic DSS colitis [Figure 3] and acute DSS colitis,[64] which further supports that CH25H knockout does not simply reduce fibrosis by diminishing overall intestinal inflammation. In line with these results, the numbers of CD4-positive cells in grafts from WT and *Ch25h* knockout animals were similar. In fact, with the antibody panel used in the CYTOF-analysis, the inflammatory infiltrate in intestinal grafts could not be distinguished between mice of both genotypes, which is well in line with involvement of CH25H in pro-fibrotic pathways independent of intestinal inflammation. However, our CYTOF analyses do not distinguish several cellular subtypes of the infiltrate. For instance, the compartment of myeloid mononuclear cells including dendritic cells [DCs] and macrophages has not been characterised in detail. Effects of macrophages on intestinal fibrosis have been demonstrated,[65,66] and our results do not exclude a modulation of frequency, activation level, and/ or phenotype of macrophages or DCs, which remains a limitation of our study.

The CH25H product 25-HC has been shown to modulate several immune responses.[21,23,25,28,29,33] 25-HC acts as an acute defence molecule and a master regulator of inflammation by increasing antiviral responses[28–30,67] and decreasing antibacterial defence mechanisms.[33,55] Our study suggests an additional role of the oxysterol 25-HC as a mediator of intestinal fibrosis. The induction of wound healing, which potentially leads to fibrosis, might thus start very early in the inflammatory cascade by the acute immune-modulatory activity of 25-HC, which is rapidly induced after an inflammatory stimulus.[68]

Despite advances in the treatment of CD-associated inflammation, a specific intestinal anti-fibrotic therapy remains an unmet clinical need.[7,8] To the best of our knowledge, no specific CH25H inhibitor is available. However, desmosterol has been shown to reduce enzymatic activity of CH25H in a seminal paper,[32] and subsequent cell culture studies[69,70] and compounds leading to desmosterol accumulation *in vivo* exist.[71] In other studies, a potential 25-HC inhibitor [LY295427, agisterol] was shown to antagonise cholesterol-homeostatic effects of 25-HC.[72,73] Finally, caffeic acid phenethyl esther [CAPE], a natural derivate from several plants as well as propolis from honey bee hives, is a powerful and specific NF-kB inhibitor[74–76] and was able to block 25-HC-mediated NF-kB activation in cell culture.[39] CAPE was able to inhibit myofibroblast formation and collagen synthesis in human fibroblasts,[39,77] animal models of hepatic fibrosis models,[78,79] and pulmonary fibrosis.[80,81]

Importantly, our experiment only addressed inhibition of the development of intestinal fibrosis, and the role of CH25H in the reversal of fibrosis remains unclear. Further, inhibition of wound healing/ fibrosis might inadvertently promote penetrating/ fistulising disease in intestinal inflammation. These concerns will have to be addressed by future animal studies.

In summary, our findings implicate the hydroxylase CH25H in intestinal fibrosis, making CH25H a potential promising novel therapeutic target to prevent intestinal fibrosis, but additional studies are required to elucidate the exact mechanism by which CH25H promotes fibrosis.

Funding

This research was supported by a grant from the Swiss National Science Foundation to BM [Grant No. 32473B_156525]; a grant from the Hartmann-Müller Foundation to BM; and an IOIBD grant to GR, MH, and BM. PHIS has been a recipient of a fellowship from the IKPP Kidney.CH under the European Unions Seventh Framework Programme for Research, Technological Development and Demonstration under the grant agreement No. 608847. The funding institutions had no role in study design, analysis, interpretation of the data, and writing of the manuscript.

Conflict of Interest

The authors declare that there are no competing interests. BM has served on a Gilead advisory board and received travelling grants and grant support from MSD. GR discloses grant support from AbbVie, Ardeypharm, MSD, FALK, Flamentera, Novartis, Roche, Tillots, UCB, and Zeller. MH discloses grant support from AbbVie and Novartis. CAW discloses grant support from Bayer and AstraZeneca.

Acknowledgments

The authors would like to thank Silvia Lang and Kirstin Atrott for technical assistance, and Matteo Berchier for the help with the image analysis algorithm.

Author Contributions

TR, MH, AWS, GR, and BM conceived of, designed, and supervised the study. TR, MH, MNGA, BW, CM, AW, and MRS performed experiments and were involved in data analysis. WTvH and GD were involved in acquisition of human data and samples. PHIS and CAW performed *in situ* hybridisation experiments. VT performed the CyTOF analysis. SL was involved in the

histological analysis. TR, MH, and BM wrote the paper. MS and GR critically revised the manuscript and added important intellectual content. All authors corrected and approved the manuscript.

Supplementary Data

Supplementary data are available at *ECCO-JCC* online.

References

1. Bernstein CN, Loftus EV Jr, Ng SC, Lakatos PL, Moum B; Epidemiology and Natural History Task Force of the International Organization for the Study of Inflammatory Bowel Disease [IOIBD]. Hospitalisations and surgery in Crohn's disease. *Gut* 2012;**61**:622–9.
2. Bemelman WA, Allez M. The surgical intervention: earlier or never? *Best Pract Res Clin Gastroenterol* 2014;**28**:497–503.
3. Gionchetti P, Dignass A, Danese S, *et al.*; ECCO. Third European evidence-based consensus on the diagnosis and management of Crohn's disease 2016. Part 2: surgical management and special situations. *J Crohns Colitis* 2017;**11**:135–49.
4. Rieder F, Fiocchi C, Rogler G. Mechanisms, management, and treatment of fibrosis in patients with inflammatory bowel diseases. *Gastroenterology* 2017;**152**:340–50.e6.
5. Gordon IO, Agrawal N, Goldblum JR, Fiocchi C, Rieder F. Fibrosis in ulcerative colitis: mechanisms, features, and consequences of a neglected problem. *Inflamm Bowel Dis* 2014;**20**:2198–206.
6. Agrawal NWE, Lopez R, Lashner B, Fiocchi C, Gordon I, Rieder F. Submucosal fibrosis in ulcerative colitis is linked with severity and chronicity of inflammation. *Gastroenterology* 2016;**150**:S575.
7. Bettenworth D, Rieder F. Reversibility of stricturing Crohn's disease - fact or fiction? *Inflamm Bowel Dis* 2016;**22**:241–7.
8. Rogler G. New therapeutic avenues for treatment of fibrosis: can we learn from other diseases? *Dig Dis* 2014;**32**[**Suppl 1**]:39–49.
9. Cosnes J, Nion-Larmurier I, Beaugerie L, Afchain P, Tiret E, Gendre JP. Impact of the increasing use of immunosuppressants in Crohn's disease on the need for intestinal surgery. *Gut* 2005;**54**:237–41.
10. Wynn TA, Ramalingam TR. Mechanisms of fibrosis: therapeutic translation for fibrotic disease. *Nat Med* 2012;**18**:1028–40.
11. Kendall RT, Feghali-Bostwick CA. Fibroblasts in fibrosis: novel roles and mediators. *Front Pharmacol* 2014;**5**:123.
12. Pohlers D, Brenmoehl J, Löffler I, *et al.* TGF-beta and fibrosis in different organs - molecular pathway imprints. *Biochim Biophys Acta* 2009;**1792**:746–56.
13. Massagué J. How cells read TGF-beta signals. *Nat Rev Mol Cell Biol* 2000;**1**:169–78.
14. Duffield JS, Grafals M, Portilla D. MicroRNAs are potential therapeutic targets in fibrosing kidney disease: lessons from animal models. *Drug Discov Today Dis Models* 2013;**10**:e127–35.
15. Hinz B. The myofibroblast: paradigm for a mechanically active cell. *J Biomech* 2010;**43**:146–55.
16. Kramann R, DiRocco DP, Humphreys BD. Understanding the origin, activation and regulation of matrix-producing myofibroblasts for treatment of fibrotic disease. *J Pathol* 2013;**231**:273–89.
17. Koga H, Yang H, Adler J, Zimmermann EM, Teitelbaum DH. Transanal delivery of angiotensin converting enzyme inhibitor prevents colonic fibrosis in a mouse colitis model: development of a unique mode of treatment. *Surgery* 2008;**144**:259–68.
18. Speca S, Rousseaux C, Dubuquoy C, *et al.* Novel PPARγ modulator GED-0507-34 levo ameliorates inflammation-driven intestinal fibrosis. *Inflamm Bowel Dis* 2016;**22**:279–92.
19. Hausmann M, Rechsteiner T, Caj M, *et al.* A new heterotopic transplant animal model of intestinal fibrosis. *Inflamm Bowel Dis* 2013;**19**:2302–14.
20. Meier R, Lutz C, Cosín-Roger J, *et al.* Decreased fibrogenesis after treatment with pirfenidone in a newly developed mouse model of intestinal fibrosis. *Inflamm Bowel Dis* 2016;**22**:569–82.
21. Gold ES, Diercks AH, Podolsky I, *et al.* 25-Hydroxycholesterol acts as an amplifier of inflammatory signaling. *Proc Natl Acad Sci U S A* 2014;**111**:10666–71.
22. Gold ES, Ramsey SA, Sartain MJ, *et al.* ATF3 protects against atherosclerosis by suppressing 25-hydroxycholesterol-induced lipid body formation. *J Exp Med* 2012;**209**:807–17.
23. Shibata N, Carlin AF, Spann NJ, *et al.* 25-Hydroxycholesterol activates the integrated stress response to reprogram transcription and translation in macrophages. *J Biol Chem* 2013;**288**:35812–23.
24. Soroosh P, Wu J, Xue X, *et al.* Oxysterols are agonist ligands of RORgammat and drive Th17 cell differentiation. *Proc Natl Acad Sci U S A* 2014;**111**:12163–8.
25. Wang F, Xia W, Liu F, Li J, Wang G, Gu J. Interferon regulator factor 1/retinoic inducible gene I [IRF1/RIG-I] axis mediates 25-hydroxycholesterol-induced interleukin-8 production in atherosclerosis. *Cardiovasc Res* 2012;**93**:190–9.
26. Lemaire-Ewing S, Berthier A, Royer MC, *et al.* 7beta-Hydroxycholesterol and 25-hydroxycholesterol-induced interleukin-8 secretion involves a calcium-dependent activation of c-fos via the ERK1/2 signaling pathway in THP-1 cells: oxysterols-induced IL-8 secretion is calcium-dependent. *Cell Biol Toxicol* 2009;**25**:127–39.
27. Dugas B, Charbonnier S, Baarine M, *et al.* Effects of oxysterols on cell viability, inflammatory cytokines, VEGF, and reactive oxygen species production on human retinal cells: cytoprotective effects and prevention of VEGF secretion by resveratrol. *Eur J Nutr* 2010;**49**:435–46.
28. Blanc M, Hsieh WY, Robertson KA, *et al.* The transcription factor STAT-1 couples macrophage synthesis of 25-hydroxycholesterol to the interferon antiviral response. *Immunity* 2013;**38**:106–18.
29. Liu SY, Aliyari R, Chikere K, *et al.* Interferon-inducible cholesterol-25-hydroxylase broadly inhibits viral entry by production of 25-hydroxycholesterol. *Immunity* 2013;**38**:92–105.
30. Xiang Y, Tang JJ, Tao W, Cao X, Song BL, Zhong J. Identification of cholesterol 25-hydroxylase as a novel host restriction factor and a part of the primary innate immune responses against hepatitis C virus infection. *J Virol* 2015;**89**:6805–16.
31. Dang EV, McDonald JG, Russell DW, Cyster JG. Oxysterol restraint of cholesterol synthesis prevents AIM2 inflammasome activation. *Cell* 2017;**171**:1057–71.e11.
32. Lund EG, Kerr TA, Sakai J, Li WP, Russell DW. cDNA cloning of mouse and human cholesterol 25-hydroxylases, polytopic membrane proteins that synthesize a potent oxysterol regulator of lipid metabolism. *J Biol Chem* 1998;**273**:34316–27.
33. Bauman DR, Bitmansour AD, McDonald JG, Thompson BM, Liang G, Russell DW. 25-Hydroxycholesterol secreted by macrophages in response to Toll-like receptor activation suppresses immunoglobulin A production. *Proc Natl Acad Sci U S A* 2009;**106**:16764–9.
34. Diczfalusy U, Olofsson KE, Carlsson AM, *et al.* Marked upregulation of cholesterol 25-hydroxylase expression by lipopolysaccharide. *J Lipid Res* 2009;**50**:2258–64.
35. Sugiura H, Koarai A, Ichikawa T, *et al.* Increased 25-hydroxycholesterol concentrations in the lungs of patients with chronic obstructive pulmonary disease. *Respirology* 2012;**17**:533–40.
36. Hannedouche S, Zhang J, Yi T, *et al.* Oxysterols direct immune cell migration via EBI2. *Nature* 2011;**475**:524–7.
37. Liu C, Yang XV, Wu J, *et al.* Oxysterols direct B-cell migration through EBI2. *Nature* 2011;**475**:519–23.
38. Esnault S, Bernau K, Torr EE, Bochkov YA, Jarjour NN, Sandbo N. RNA-sequencing analysis of lung primary fibroblast response to eosinophil-degranulation products predicts downstream effects on inflammation, tissue remodeling and lipid metabolism. *Respir Res* 2017;**18**:188.
39. Ichikawa T, Sugiura H, Koarai A, *et al.* 25-hydroxycholesterol promotes fibroblast-mediated tissue remodeling through NF-κB dependent pathway. *Exp Cell Res* 2013;**319**:1176–86.
40. Faul F, Erdfelder E, Lang AG, Buchner A. G*Power 3: a flexible statistical power analysis program for the social, behavioral, and biomedical sciences. *Behav Res Methods* 2007;**39**:175–91.

41. Becker C, Fantini MC, Neurath MF. High resolution colonoscopy in live mice. *Nat Protoc* 2006;**1**:2900–4.
42. Obermeier F, Kojouharoff G, Hans W, Schölmerich J, Gross V, Falk W. Interferon-gamma [IFN-gamma]- and tumour necrosis factor [TNF]-induced nitric oxide as toxic effector molecule in chronic dextran sulphate sodium [DSS]-induced colitis in mice. *Clin Exp Immunol* 1999;**116**:238–45.
43. Leeb SN, Vogl D, Falk W, Schölmerich J, Rogler G, Gelbmann CM. Regulation of migration of human colonic myofibroblasts. *Growth Factors* 2002;**20**:81–91.
44. Nimmons D, Limdi JK. Elderly patients and inflammatory bowel disease. *World J Gastrointest Pharmacol Ther* 2016;**7**:51–65.
45. Butter M, Weiler S, Biedermann L, *et al.* Clinical manifestations, pathophysiology, treatment and outcome of inflammatory bowel diseases in older people. *Maturitas* 2018;**110**:71–8.
46. Viñuela A, Brown AA, Buil A, *et al.* Age-dependent changes in mean and variance of gene expression across tissues in a twin cohort. *Hum Mol Genet* 2018;**27**:732–41.
47. Luu W, Sharpe LJ, Capell-Hattam I, Gelissen IC, Brown AJ. Oxysterols: old tale, new twists. *Annu Rev Pharmacol Toxicol* 2016;**56**:447–67.
48. Lawrance IC, Rogler G, Bamias G, *et al*. Cellular and molecular mediators of intestinal fibrosis. *J Crohns Colitis* 2017;**11**:1491–503.
49. Rieder F, Fiocchi C. Intestinal fibrosis in IBD – a dynamic, multifactorial process. *Nat Rev Gastroenterol Hepatol* 2009;**6**:228–35.
50. Latella G, Rogler G, Bamias G, *et al.* Results of the Fourth Scientific Workshop of the ECCO [I]: pathophysiology of intestinal fibrosis in IBD. *J Crohns Colitis* 2014;**8**:1147–65.
51. Melgar S, Karlsson A, Michaëlsson E. Acute colitis induced by dextran sulfate sodium progresses to chronicity in C57BL/6 but not in BALB/c mice: correlation between symptoms and inflammation. *Am J Physiol Gastrointest Liver Physiol* 2005;**288**:G1328–38.
52. Breynaert C, Dresselaers T, Perrier C, *et al.* Unique gene expression and MR T2 relaxometry patterns define chronic murine dextran sodium sulphate colitis as a model for connective tissue changes in human Crohn's disease. *PLoS One* 2013;**8**:e68876.
53. Suzuki K, Sun X, Nagata M, *et al.* Analysis of intestinal fibrosis in chronic colitis in mice induced by dextran sulfate sodium. *Pathol Int* 2011;**61**:228–38.
54. Kiesler P, Fuss IJ, Strober W. Experimental models of inflammatory bowel diseases. *Cell Mol Gastroenterol Hepatol* 2015;**1**:154–70.
55. De Salvo C, Ray S, Pizarro TT. Mechanisms and models for intestinal fibrosis in IBD. *Dig Dis* 2014;**32[Suppl 1]**:26–34.
56. Lutz C, Weder B, Hünerwadel A, *et al.* Myeloid differentiation primary response gene [MyD] 88 signalling is not essential for intestinal fibrosis development. *Sci Rep* 2017;**7**:17678.
57. Xu L, Bai Q, Rodriguez-Agudo D, *et al.* Regulation of hepatocyte lipid metabolism and inflammatory response by 25-hydroxycholesterol and 25-hydroxycholesterol-3-sulfate. *Lipids* 2010;**45**:821–32.
58. Palozza P, Simone A, Catalano G, *et al*. Lycopene prevention of oxysterol-induced proinflammatory cytokine cascade in human macrophages: inhibition of NF-kappaB nuclear binding and increase in PPARgamma expression. *J Nutr Biochem* 2011;**22**:259–68.
59. Reboldi A, Dang EV, McDonald JG, Liang G, Russell DW, Cyster JG. Inflammation. 25-Hydroxycholesterol suppresses interleukin-1-driven inflammation downstream of type I interferon. *Science* 2014;**345**:679–84.
60. Reboldi A, Cyster JG. Peyer's patches: organizing B-cell responses at the intestinal frontier. *Immunol Rev* 2016;**271**:230–45.
61. Wilson MS, Madala SK, Ramalingam TR, *et al.* Bleomycin and IL-1beta-mediated pulmonary fibrosis is IL-17A dependent. *J Exp Med* 2010;**207**:535–52.
62. Tan Z, Qian X, Jiang R, *et al.* IL-17A plays a critical role in the pathogenesis of liver fibrosis through hepatic stellate cell activation. *J Immunol* 2013;**191**:1835–44.
63. Biancheri P, Pender SL, Ammoscato F, *et al*. The role of interleukin 17 in Crohn's disease-associated intestinal fibrosis. *Fibrogenesis Tissue Repair* 2013;**6**:13.
64. Wyss A, Raselli T, Perkins N, *et al.* The EBI2-oxysterol axis promotes the development of intestinal lymphoid structures and colitis. *Mucosal Immunol* 2019;**11**:1.
65. Salvador P, Macías-Ceja DC, Gisbert-Ferrándiz L, *et al.* CD16+ macrophages mediate fibrosis in inflammatory bowel disease. *J Crohns Colitis* 2018;**12**:589–99.
66. Kühl AA, Erben U, Kredel LI, Siegmund B. Diversity of intestinal macrophages in inflammatory bowel diseases. *Front Immunol* 2015;**6**:613.
67. Pezacki JP, Sagan SM, Tonary AM, *et al.* Transcriptional profiling of the effects of 25-hydroxycholesterol on human hepatocyte metabolism and the antiviral state it conveys against the hepatitis C virus. *BMC Chem Biol* 2009;**9**:2.
68. Park K, Scott AL. Cholesterol 25-hydroxylase production by dendritic cells and macrophages is regulated by type I interferons. *J Leukoc Biol* 2010;**88**:1081–7.
69. Wang JH, Tuohimaa P. Regulation of cholesterol 25-hydroxylase expression by vitamin D3 metabolites in human prostate stromal cells. *Biochem Biophys Res Commun* 2006;**345**:720–5.
70. Tsujioka T, Yokoi A, Itano Y, *et al.* Five-aza-2'-deoxycytidine-induced hypomethylation of cholesterol 25-hydroxylase gene is responsible for cell death of myelodysplasia/leukemia cells. *Sci Rep* 2015;**5**:16709.
71. Sachs BA, Wolfman L. 20, 25-Diazacholestenol dihydrochloride. Inhibition of cholesterol biosynthesis in hyperlipemic subjects. *Arch Intern Med* 1965;**116**:366–72.
72. Bielska AA, Olsen BN, Gale SE, *et al.* Side-chain oxysterols modulate cholesterol accessibility through membrane remodeling. *Biochemistry* 2014;**53**:3042–51.
73. Janowski BA, Shan B, Russell DW. The hypocholesterolemic agent LY295427 reverses suppression of sterol regulatory element-binding protein processing mediated by oxysterols. *J Biol Chem* 2001;**276**:45408–16.
74. Natarajan K, Singh S, Burke TR Jr, Grunberger D, Aggarwal BB. Caffeic acid phenethyl ester is a potent and specific inhibitor of activation of nuclear transcription factor NF-kappa B. *Proc Natl Acad Sci U S A* 1996;**93**:9090–5.
75. Watabe M, Hishikawa K, Takayanagi A, Shimizu N, Nakaki T. Caffeic acid phenethyl ester induces apoptosis by inhibition of NFkappaB and activation of Fas in human breast cancer MCF-7 cells. *J Biol Chem* 2004;**279**:6017–26.
76. McEleny K, Coffey R, Morrissey C, Fitzpatrick JM, Watson RW. Caffeic acid phenethyl ester-induced PC-3 cell apoptosis is caspase-dependent and mediated through the loss of inhibitors of apoptosis proteins. *BJU Int* 2004;**94**:402–6.
77. Mia MM, Bank RA. The pro-fibrotic properties of transforming growth factor on human fibroblasts are counteracted by caffeic acid by inhibiting myofibroblast formation and collagen synthesis. *Cell Tissue Res* 2016;**363**:775–89.
78. Li M, Wang XF, Shi JJ, *et al.* Caffeic acid phenethyl ester inhibits liver fibrosis in rats. *World J Gastroenterol* 2015;**21**:3893–903.
79. Tomur A, Kanter M, Gurel A, Erboga M. The efficiency of CAPE on retardation of hepatic fibrosis in biliary obstructed rats. *J Mol Histol* 2011;**42**:451–8.
80. Zaeemzadeh N, Hemmati A, Arzi A, Jalali M, Rashidi I. Protective effect of caffeic acid phenethyl ester [CAPE] on amiodarone-induced pulmonary fibrosis in rat. *Iran J Pharm Res* 2011;**10**:321–8.
81. Sezer M, Sahin O, Solak O, Fidan F, Kara Z, Unlu M. Effects of caffeic acid phenethyl ester on the histopathological changes in the lungs of cigarette smoke-exposed rabbits. *Basic Clin Pharmacol Toxicol* 2007;**101**:187–91.